Proceedings of HT2007
2007 ASME-JSME Thermal Engineering Summer Heat Transfer Conference
July 8-12, 2007, Vancouver, British Columbia, CANADA

HT2007-32674

ATOMISTIC VISUALIZATION OF BALLISTIC PHONON TRANSPORT

Neil Zuckerman Jennifer R. Lukes

University of Pennsylvania
Dept. of Mechanical Engineering and Applied Mechanics
Philadelphia, PA, USA

ABSTRACT

Heat transfer in solid materials at short time scales, short length scales, and low temperatures is governed by the transport of ballistic phonons. In anisotropic crystals, the energy carried by these phonons is strongly channeled into well-defined directions in a phenomenon known as phonon focusing. Presented here is a new molecular dynamics simulation approach for visualizing acoustic phonon focusing in anisotropic crystals. An advantage of this approach over experimental phonon imaging techniques is that it allows examination of phonon propagation at selected modes and frequencies. The spatial, mode, and frequency dependence of ballistic energy transport gained with this approach will be useful for understanding heat transfer issues in high frequency electronics and short time scale laser-material interactions.

NOMENCLATURE

k	wave number
k	wave vector
KE	kinetic energy
NCX	number of lattice cells used in *x* direction
NCY	number of lattice cells used in *y* direction
NCZ	number of lattice cells used in *z* direction
r	radial position, from source
t	time
$\mathbf{v_g}$	group velocity vector
x	coordinate direction
y	coordinate direction, lateral
z	coordinate direction, lateral
ω	vibrational angular frequency

INTRODUCTION

The transfer of heat within non-metallic solids occurs primarily by the propagation of elastic waves associated with the displacement of atoms from their lattice sites. These traveling vibrational waves occur in spatially localized, quantized units called phonons. In single crystals at low temperatures the phonons may travel ballistically, meaning they persist along straight-line trajectories for long distances without destruction or redirection. The elastic anisotropy of crystals causes directional variation in this ballistic heat flux, channeling higher numbers of phonons along specific directions. Understanding how a material preferentially channels phonons along various directions will provide a better understanding of heat transfer in crystals and material properties, with increased utility for applications involving short heat pulses and/or low temperatures. The visualization of this heat propagation can also improve understanding and modeling of low-temperature heat transfer at greater length and time scales when material properties yield different speeds of heat propagation in different directions, as these directional variations influence the mesoscale transport of phonons.

The phonon-focusing behaviors of crystals have been experimentally investigated for a limited selection of materials in laboratory settings, such as Si, GaAs, LiF, InSb, Ge, and other semiconductors [1]. The techniques measure heat pulse intensity at various positions on a crystal surface following excitation of phonons from a point source on the opposite side. The point source is commonly excited by a narrow electron beam or a laser briefly impinging on a metal surface film. The material sample is maintained at a low temperature (e.g. 2 K) to suppress phonon-phonon collisions and diffusive transport of heat. The signal on the crystal surface is commonly picked up by superconducting detectors which change resistance in response to temperature increases [1, 2]. Input pulse durations are on the order of 10 nanoseconds which requires careful tracking of time or phase differences between the heat pulse input and signal output. The equipment and high-quality material samples necessary for this method make a numerical method a desirable alternative.

The observed behavior of the materials can be explained using principles of elasticity for crystalline lattice structures. In general, the wave vector and the group velocity vector (propagation direction) of an elastic wave in a crystal will have different directions. Due to crystal anisotropy, two separate phonons with wave vectors possessing different magnitude and direction may have parallel group velocity vectors. This is illustrated in Figure 1 which shows a slowness contour (line of constant ω) in a two-dimensional momentum space, corresponding to phase velocities of a transverse mode in a (100) face plane of a cubic crystal [3]. Group velocity vectors will be perpendicular to this slowness surface. The two wavevectors (**k**) shown in the figure have identical group velocity vectors ($\mathbf{v_g}$). A collection of phonons of a given polarization with uniform density in wave vector space will have real-space group velocity vectors with a non-uniform distribution, resulting in real-space directions with higher- and lower-than-average phonon fluxes, as shown in Figure 2. The aspherical wave front surface surrounding a point source of phonons may feature "caustics," directions or surfaces which have been experimentally observed to have very high phonon fluxes (phonon focusing). Up to three distinct acoustic vibrational eigenmodes will be present in any given direction. The mode with the highest velocity (and lowest "slowness" k/ω) is labeled quasi-longitudinal, and along crystal axes will have the form of a pure longitudinal vibration. Similarly the other two vibrational modes are labeled quasi-slow transverse and quasi-fast transverse based on their velocities, and along the axes of crystal alignment will be pure transverse vibrations. In other directions a vibrational eigenmode will be a mixed mode. Each of the distinct vibrational eigenmodes of the lattice will have a different group velocity (a function of direction) and a different wave front surface.

The most common method of numerical investigation uses a Monte Carlo model of phonon transport to simulate the experimental technique [4]. The Monte Carlo simulation performs calculations for many phonons in a selected range of wavevector and of selected polarizations to determine their position and time of arrival on the crystal surface corresponding to the image plane. Many individual phonon transport calculations are required to span the necessary time interval, densely sample all relevant wave number directions, and accumulate enough phonons on the image plane within a given time window to provide clear contrast (dynamic range and signal resolution). The more detailed versions of these Monte Carlo models incorporate the full three-dimensional dispersion relations to calculate phonon group velocities.

In this study, Molecular Dynamics (MD) is explored as a tool for visualizing spatially-nonuniform propagation of heat in crystal lattices. It serves as an alternative to the Monte Carlo method and other numerical models. Unlike the Monte Carlo approach, the established MD models of various materials incorporate potential energy functions to describe their atomic interactions. This means that the user need not compute dispersion relations or material elastic stiffness constants, because these properties are natural results of the selected potential function.

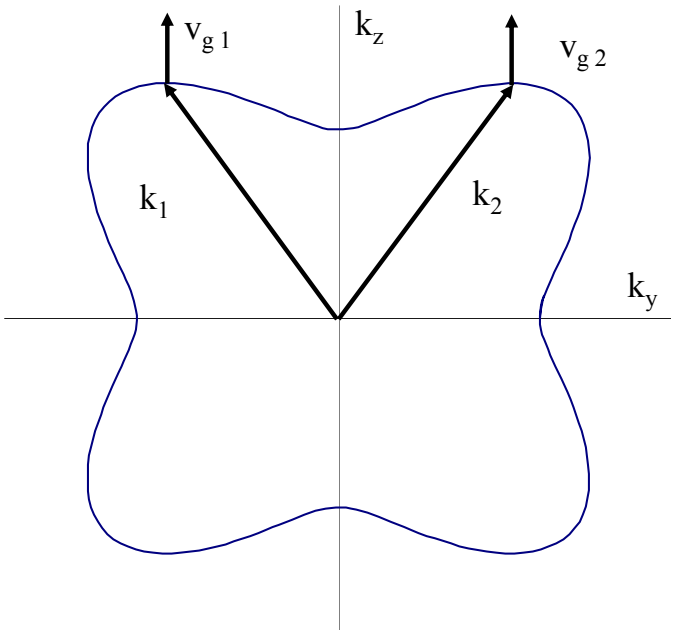

Figure 1: Slowness surface for quasi-transverse mode in (100) plane, plotted in k-space with sample wave and group velocity vectors

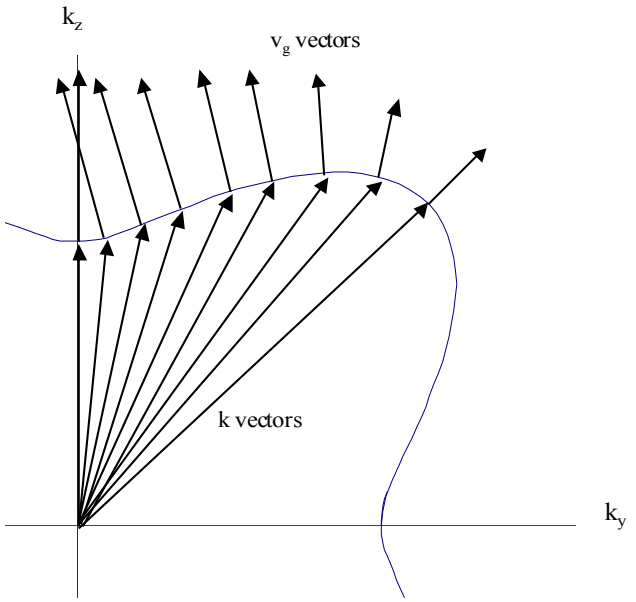

Figure 2: Schematic depiction of nonuniform distribution of group velocity vectors resulting from uniform distribution of wave vectors

SIMULATION METHOD

The simulation approach is to model a block of atoms, impose a point-source vibration into the atomic lattice, and then monitor atoms on a selected crystal plane to determine their kinetic energy as a function of position and time. This method is selected because of its similarity to the experimental technique.

The molecular dynamics model used is based on program code of Lukes and Tien [5]. This solid inert-gas model was selected based on its speed of computation. The selected Lennard-Jones 12-6 potential model [6] gives cubic stiffness constants for argon with ratios close to those of GaAs, a semiconductor material used in several phonon imaging experiments [7, 8], which allows us to make comparisons between MD model results and experimental images. The model simulates a solid argon crystal in a face-centered cubic lattice, which supports acoustic modes only. The lattice is configured as a large box-shaped domain with rigid walls on two opposite sides and periodic boundaries on the other four sides (Figure 3). The simulation domain typically contains between 5,000 and 340,000 atoms, with side lengths of up to 26 nm, based on 50 unit cells sized at 0.53 nm each.

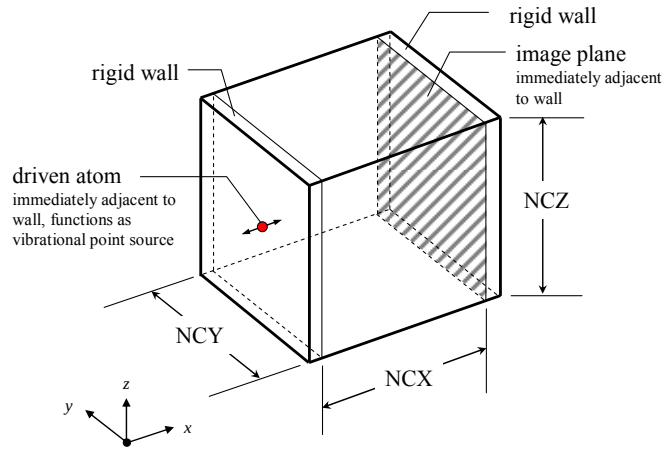

Figure 3: Schematic of Simulation Domain

A plane of atoms adjacent to the far wall of the simulation domain is identified as the "image plane." The position and velocity of each atom in the image plane is tracked over time, potentially at every time step. In the computations described below, these data are recorded at intervals of 10 or 50 time steps, where each time step represents 1 fs. To provide very high time resolution they could be sampled every time step, which would generate a very large data set for post-processing. The recorded velocity of each atom is used to compute the kinetic energy at the image plane as a function of position. Using this method one could also track and plot momentum, if desired, for comparison versus experimental sensors which respond to phonon momentum rather than energy.

The lattice in the model is first initialized at a temperature of 0K. A point source of heat is generated by moving a single atom in a lattice position centered on one wall of the model. This generates disturbances in the positions of neighboring atoms which travel in a wavelike fashion radially away from the point source. By moving the atom in particular directions one can generate waves or combinations of waves with selected polarizations. The most successful point-source motions we have used thus far have the shape of a narrow wave packet, examples of which are shown in Figure 4. The packet amplitude represents displacement of the driving atom from its equilibrium position, and the time derivative of the packet is proportional to the magnitude of the local atomic velocity. The kinetic energy of the moving atom then varies over time as shown in Figure 5, with individual peaks in kinetic energy at successive time intervals. This pattern of distinct peaks is preserved as the excited wave travels away from the source and reaches the image plane. After the packet reaches the far wall adjacent to the image plane, it reflects and travels back towards the driven atom. The result is that the kinetic energy of each point (each atom) on the image plane has a sequence of peaks resembling those in Figure 5, and for sufficiently high NCX will return to a low-temperature state after the complete wave packet has arrived and reflected. Due to different points on the image plane having different distances from the source, and due to the directional variation of group velocity, the observed effect is that of a series of pulses arriving at the center of the *y-z* image plane and traveling radially outward in a series of rings.

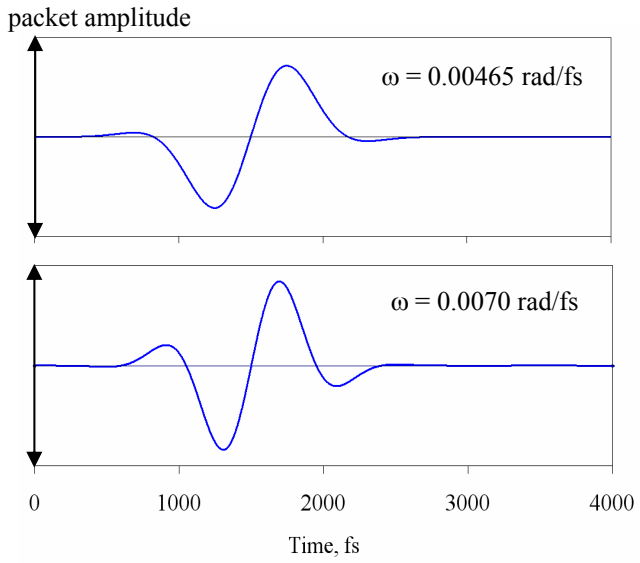

Figure 4: Typical narrow wave packet shapes, ω=0.00465 and ω=0.0070 rad/fs

The use of a temporal wave packet allows the input to match a selected phonon frequency ω, which is a useful numerical model feature not available in the experimental method. The direction of the particle velocity is chosen, and the resulting wavenumbers and group velocities of excited vibrations are generated within the model as a consequence of the crystal stiffness constants, determined by the lattice structure and potential function. To extract information about particular phonons it is desirable to excite vibrations primarily of a single polarization, and this is possible by selecting directions of source atom motion that are aligned with the crystal axes. Input wave packet amplitude should be kept small to keep the material response in the linear regime (e.g. 1% of a lattice constant). Due to the $1/r^2$ decay of vibrational energy propagating from a point source in three dimensions [3], excessively small displacements will be difficult to distinguish at the image plane. In practice the motion of a single atom will result in waves of more than one polarization, but along crystal axes the majority of the wave energy will fall into one particular mode.

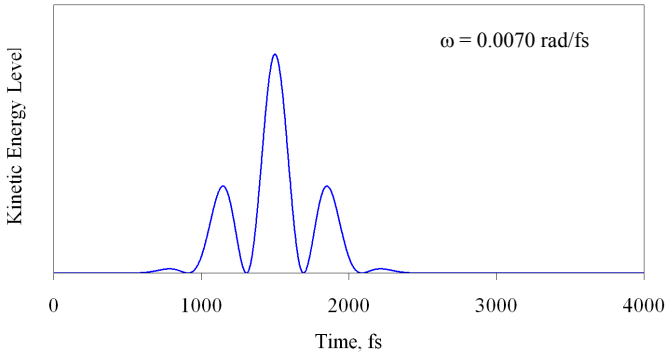

Figure 5: Kinetic energy time history of wave packet, , ω=0.0070 rad/fs

The inclusion of periodic boundaries on the sides of the model could potentially clutter the image plane signal with periodic "duplicates" of the initial pulse, formed by wave fronts that travel to one periodic boundary, wrap around to the opposing periodic boundary, and eventually arrive at the image plane. To prevent this confusing effect, the model is constructed such that the distance between the fixed walls in the *x* direction is in the range of 50-70% of the distance between opposing periodic boundaries in the *y* and *z* directions. Data is sampled for a limited time and over a limited span of the image plane to filter out any stray signals that may have passed through periodic boundaries on their way to the image plane.

RESULTS AND DISCUSSION

Computations are performed for two types of input polarization. In the first case, the input vibration is aligned with the x-axis to give a primarily longitudinal pulse. The motion of the point-source atom is defined by a wave packet, which results in multiple bands of kinetic energy appearing on the image plane, corresponding to peaks and valleys of the wave packet. The patterns on the image plane are examined to isolate those associated with the quasi-longitudinal wave front, that which contains the majority of the wave energy.

Figure 6 shows the wave front pattern generated by this longitudinal displacement packet. The squared-off rather than circular shape is a direct consequence of the directional variation of the speed of sound. This pattern is repeatable for simulation domains with differing ratios of sizes in the *y* and *z* directions. The wave-packet nature of the driving vibration results in a pulse that is spread out in space on the image plane. The outline of the wave front on the image plane is that of a circle stretched in the *y*-*z* diagonal directions. The shape is similar to quasi-longitudinal wave front lines shown experimentally in [7,8].

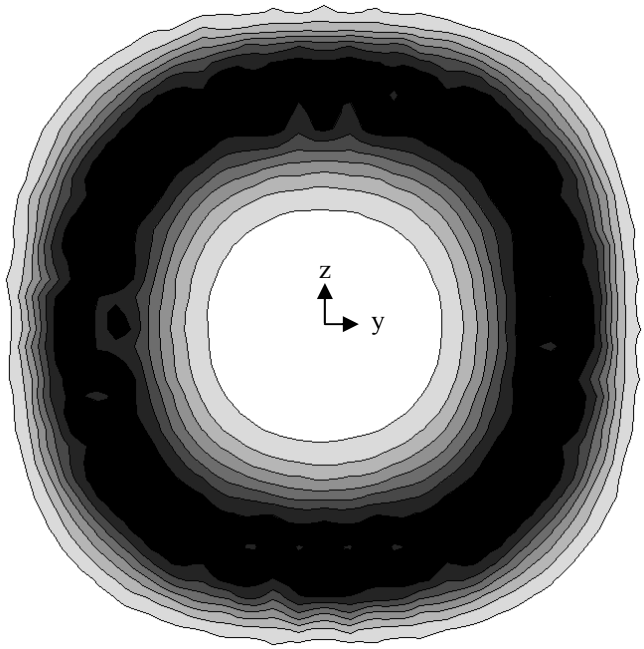

Figure 6: Kinetic energy pattern on image plane, x-axis longitudinally-polarized pulse, 12×18×34 domain, t = 4.7 ps, ω=0.00465 rad/fs

Figure 7 shows a time-history of the wave front of a longitudinal-driven pulse expanding across the image plane, corresponding to a single peak of the wave packet. The vertical lines are drawn at the edges of the crystal. The images use slightly different contour scales due to the selection of a single packet envelope which must cause small variations in packet maximum amplitude. As seen in experiments, the pulse

appears to emerge from a central point, and then appears to travel radially outwards in the *y*-*z* plane, forming a rounded-square shape. The intensity of the contours indicates energy density per unit of crystal surface area.

The ballistic phonons are not actually traveling in a lateral direction in the *y*-*z* plane, but rather along radial lines emanating from the point source of energy on the opposite side of the crystal. It is conceptually more correct to describe the three-dimensional position of a wave front corresponding to an energy peak of the packet, with the image on the plane being the intersection of this wave front and a planar surface. The radial motion apparent in the *y*-*z* plane is the motion of the intersection of the wave front and the *y*-*z* plane, and thus the velocity of an image feature in this plane is only a projection of the propagation velocity of the image feature on the expanding wave front. This is further illustrated in the two-dimensional schematic of Figure 8, showing a section cut through a crystal, with an expanding aspherical wave front contacting a fixed image plane at successive times. From the image seen in Figure 6 we can see that the energy traveling from a point source in an FCC crystal propagates at higher speeds in the diagonal directions, those with group velocity vectors closer to the [111] direction in which the lattice has the greatest stiffness.

The second type of input polarization is a transverse polarization in the *y*-*z* plane. The model is run multiple times with the same simulation domain but using different polarization vectors in the *y*-*z* plane. Atomic displacement distances are adjusted taking into account the crystal elastic stiffness along the various directions, in order to invest the same amount of vibrational energy at the point source for different models with different directions of motion. Directional stiffness is calculated per [9] using the 12-6 argon data of Barker *et al.* [10]. The experimental distribution of transverse waves with polarization in the *y*-*z* plane spans a range of directions of group velocity vectors. The driving atom used as the point source in the model is only allowed to travel along a single axis of motion in the *y*-*z* plane, which naturally generates azimuthally non-uniform contours in the image plane. To adjust for this difference between the experimental distribution of wave vector ***k***, and that used in a single model, a series of sixteen models are added together. Each model has the transverse polarization direction progressively shifted by $\pi/8$ radians in the *y*-*z* plane, relative to the previous model. The sum of the these individual runs represents the image expected from a group of transversely-polarized phonons with a uniform (random) distribution of wave vector alignment in the *y*-*z* plane.

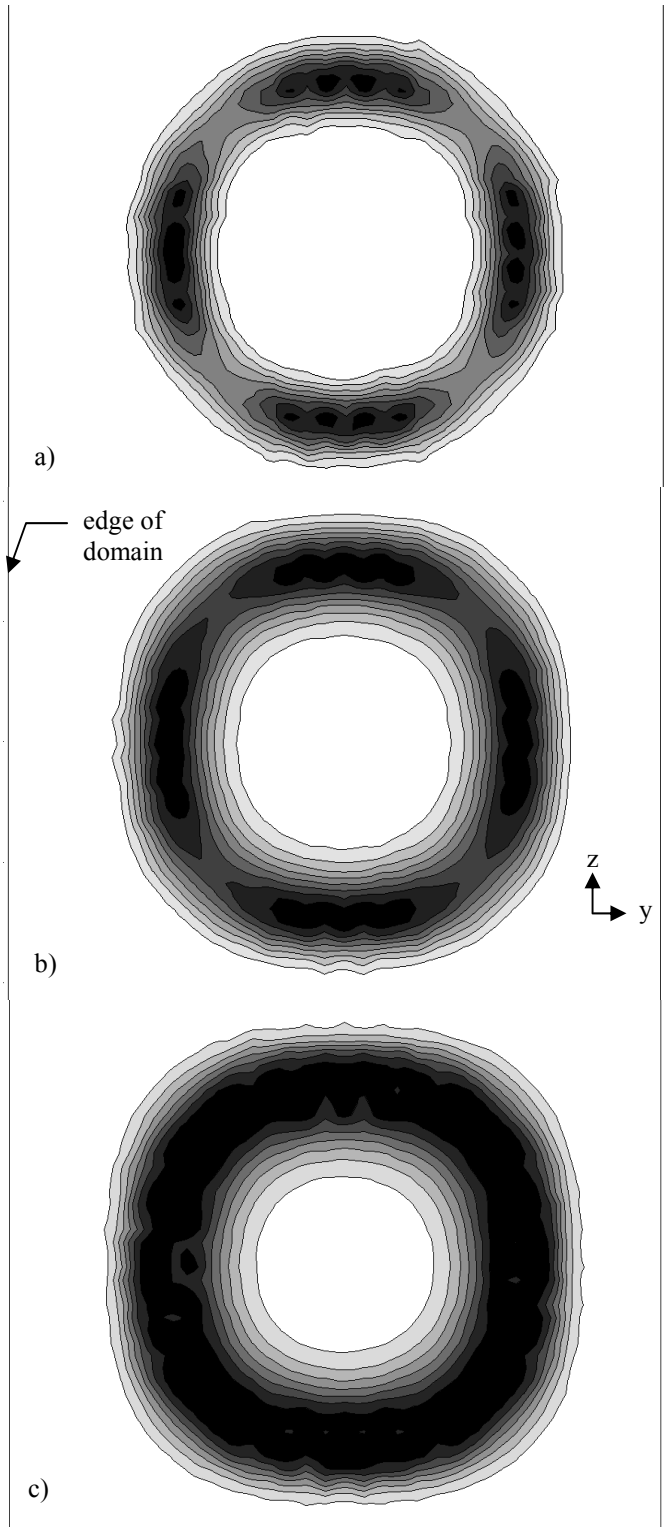

Figure 7 a-c: Kinetic energy contours - progressive time images of expanding longitudinal pulse, 12×18×34 cell domain, *t* = 4.5 ps (a), 4.6 ps (b), 4.7 ps (c), ω=0.00465 rad/fs (slightly different contour scales)

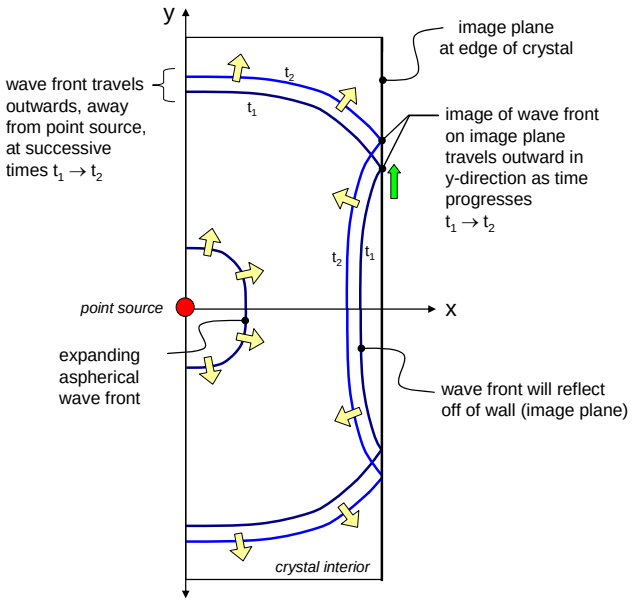

Figure 8: Two-dimensional schematic of wave fronts intersecting image plane at successive times

Figure 9 shows the composite wave front pattern generated by the transverse wave inputs. The input disturbances generated both transverse and longitudinal waves, an unavoidable consequence of the lattice structure and the three stiffness constants. At the selected time, diagonal lines at 45 degrees to the crystal axes are visible. These are associated with focusing of energy due to the quasi-fast transverse pulses. The four oval-shaped regions of high energy do not directly match experimental images; they are due to longitudinal wave energy present and due to differences between the continuous experimental and the discrete simulated directional spectra of **k**. The discrete, limited resolution of the MD model requires curve fitting to generate contours, and can make some features difficult to visualize, but the diagonal contour lines match the location shown in experimental measurements on GaAs [7, 8].

Images at different vibrational frequencies can be produced by running the model with similar wave packets of differing frequencies (c.f. Figure 4). Dispersion of the wave packet may be examined by measuring the width of the packet sensed in the image plane. Two packets generated at different frequencies, ω=0.007 rad/fs and ω=0.011 rad/fs, but with the same envelope width and envelope center synchronization, arrive at the image plane at different times due to their difference in group velocities. In addition, the packets are stretched out in time. The ω=0.007 rad/fs packet signal, shown in Figure 10 and generated using the position input profile displayed in Figure 4, had a full-width half-maximum of 1.0 ps. In comparison, the ω=0.011 rad/fs packet had a full-width half-maximum of 1.3 ps.

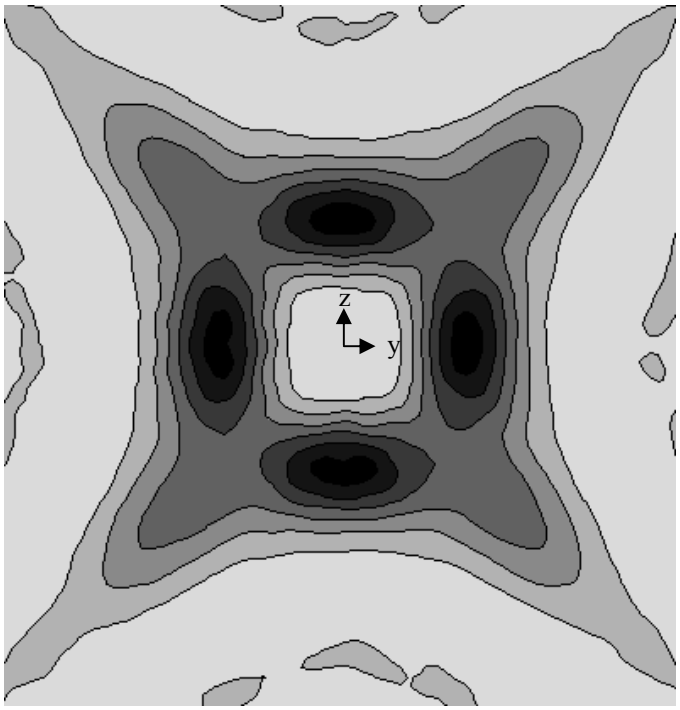

Figure 9: Kinetic energy pattern on image plane, source driven with y-z transverse polarizations, , 12×20×20 cell domain, t = 8.5 ps, ω=0.0066 rad/fs

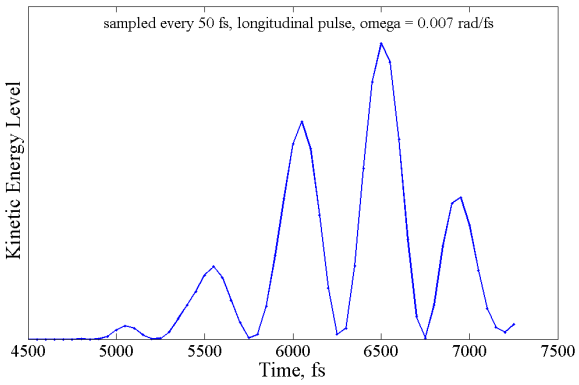

Figure 10: Time history of kinetic energy at the center of the image plane, longitudinal pulse, ω=0.007 rad/fs

As shown by the shaded regions on the dispersion relation in Figure 11, two packets with similar frequency span $\Delta\omega$ will have different wave number span Δk and different ranges of group velocity. Narrow wave packets generated for these high k span a wider range of k and have a range of propagation speed due to dispersion. The packet then becomes distorted as it travels, and the spatial distribution of energy seen on the image plane becomes even more uneven.

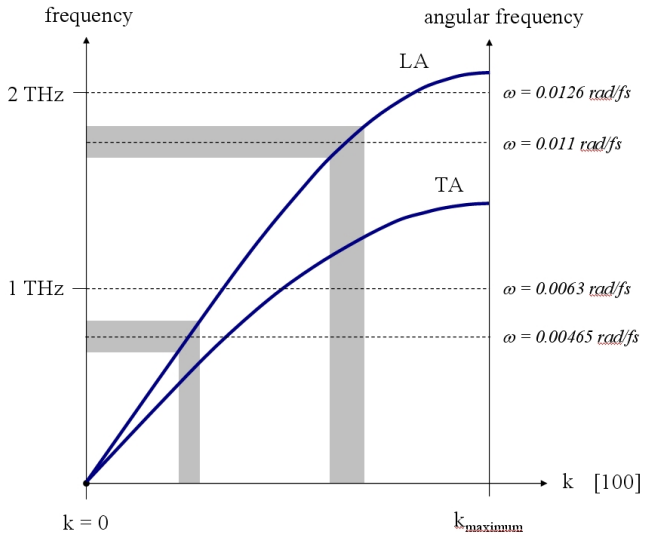

Figure 11: 12-6 Argon dispersion relation for [100] direction, based on Barker *et al.* (reference [10])

SIMULATION ARTIFACTS PRESENT AT LATE TIMES

Figure 12 and Figure 13 present a pair of images with data sampled at very late times, well after the wave fronts have traveled through periodic boundaries. The packet-shaped pulse results in multiple "islands" of high kinetic energy, rather than continuous streaks. Figure 12, from a model using 10 × 14 × 14 cells, shows patterns near the corners of the image that suggest some degree of phonon focusing. Figure 13 shows the model with the same initial conditions, run on a 10 × 22 × 14 cell domain. Both figures are colored using the same contour scale. Some patterns near the center of the figures are similar, but there are apparent differences between the corners of Figure 12 and the same regions shown in Figure 13. These features are distorted by periodic overlaps of waves and do not represent valid phonon focusing patterns. In addition, at sufficiently late time steps the model may display pulses that have reflected off of both fixed walls and returned to the image plane a second time. These two effects limit the total simulation time over which meaningful images will be present. For the method to produce proper results the patterns must be shown to be invariant to lateral extensions of the simulation domain, and short time window(s) used must be limited to avoid picking up the overlapping periodic signals. The model should be run with various simulation domain shapes to verify that the patterns of interest are not domain-dependent.

The resulting data set contains local kinetic energy levels as a function of position and time (KE = f(y,z,t)) which may be post-processed as desired. The data from a range of times may be added (integrated) to simulate a time window corresponding to that of an experimental sensor circuit. The images shown herein are contour maps of kinetic energy at selected instants, plotted with a cubic spline curve fit.

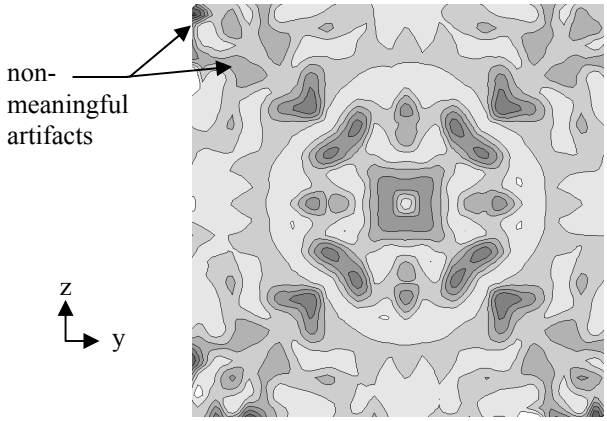

Figure 12: Kinetic energy contours in the image plane, 10 × 14 × 14 cell model, t = 12 ps - contains energy transmitted through periodic boundaries, showing simulation artifacts

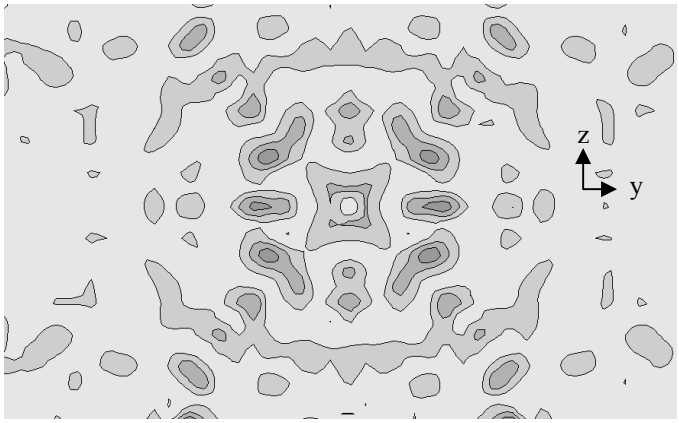

Figure 13: Kinetic energy contours in the image plane, 10 × 22 × 14 cell model, t =12 ps - contains energy transmitted through periodic boundaries, showing simulation artifacts

Given a sufficiently large model, one could select a multiple-atom region of the material to serve as the point source of phonons. In this surface region the atoms could be given initial velocities based on a chosen temperature profile (e.g. Planck distribution), and then allowed to interact over time and redistribute the energy by ballistic transport. This approach would more closely match that of the experiment. To maintain the ratio of the heated region diameter to material sample size found in the experiment, the model would have to incorporate millions of atoms. This desirable but computationally expensive method is beyond the scope of the present calculations.

ADVANTAGES AND LIMITATIONS OF THE METHOD

A key advantage of the present approach is that it eliminates the task of directly calculating the dispersion relation or vibrational eigenvectors and eigenvalues for every possible

direction. Instead, this information results naturally from the choice of potential function.

The modeling technique relies on selection of domain size in the *y*-*z* plane (NCY × NCZ as shown in Figure 3) to provide sufficient resolution of the phonon images. This feature is also common to the Monte Carlo model, where the image plane is sampled into bins which collect incident phonons. This model resolves signal level as a scalar value inherent at every step of the calculation, so runs containing many phonons are not necessary, unlike the Monte Carlo approach. Instead, the MD approach requires selection of simulation cell length in the *x* direction to provide the proper angular span of group velocity vector directions, and this translates the *y*-*z* resolution into an angular resolution. As the length of the model increases in the *x* direction (NCX), the computation time rises in proportion to NCX^2, due to a linear increase in the number of atoms modeled combined with a linear increase in the simulated time required for a pulse to ballistically traverse the simulation domain, traveling from the source to the image plane. This scaling relation is expected to make the MD model computationally expensive for high resolution/large domain simulations.

In the Monte Carlo approach, a large number of phonons and hence individual computations are necessary to ensure sufficient *y* resolution, *z* resolution, time resolution (via window selection), and image contrast or relative intensity. Increasing any one of these can proportionally increase computation time. Increasing the number of points in the Monte Carlo model's *y*-*z* plane fourfold while maintaining the same angular spread will require four times the computation time. In the MD model, maintaining a given angular span of group velocity vectors while increasing the *y*-*z* plane's pixel count (resolution) fourfold will require doubling NCX, NCY, NCZ, and simulated time, ultimately requiring sixteen times the computation time. This potentially high cost of the MD model is somewhat compensated for by the collection of data with very high time resolution, and with very high signal level resolution in the image plane by using floating-point values for kinetic energy levels.

The figures created in this study were taken from runs using domains of at least 12×20×18 unit cells. Smaller computational domains gave indistinct patterns due to poor resolution. Computations were completed with domains as large as 30×50×50 which occupied a single processor for two days. A model of this type using 12-6 argon potential functions, could produce results for a 60×100×100 cell case in less than a month using a single processor available today. While increased domains will provide higher resolution they also result in decreased pulse amplitude at the image plane, thus lower signal-to-noise levels. As the pulse propagates over a longer distance it is subject to increased scattering due to anharmonic potential functions, and raising the initial pulse amplitude to increase signal levels will distort the pulse by increasing the anharmonic scattering. Though it would also affect the resolution, a pulse driven using multiple atoms would improve the signal-to-noise level.

CONCLUSIONS

A new MD method was developed to observe ballistic phonon propagation in crystals. It revealed anisotropic propagation of wave fronts associated with point-source energy inputs using narrow wave packets. These wave front images showed focusing patterns associated with the quasi-longitudinal and quasi-fast transverse wave modes. This method may serve as an alternative to experimental and other numerical methods due to its potentially high time resolution, high signal resolution, and ability to simulate vibrations of a specific frequency.

ACKNOWLEDGMENTS

This work was supported by National Science Foundation CAREER grant no. CBET-0547588.

REFERENCES

[1] Wolfe, J. P., 1998, *Imaging Phonons: Acoustic Wave Propagation in Solids*, Cambridge University Press.

[2] Shields, J. A., Tamura, S., and Wolfe, J. P., 1991, "Elastic Scattering of Acoustic Phonons in Si," Physical Review B **43** (6), pp4966-4975.

[3] Auld, B. A., 1973, *Acoustic Fields and Waves in Solids, Volume I*, John Wiley & Sons, New York.

[4] Gańcza, W. M. and Paszkiewicz, T., 1995, "Phonon Focussing Patterns: Monte Carlo Simulation of the Motion of Ballistic Phonon Beams in Cubic Crystals," Computer Physics Communications **85**, pp423-436.

[5] Lukes, J. R., and Tien, C.-L., 2004, "Molecular Dynamics Simulation of Thermal Conduction in Nanoporous Thin Films," Microscale Thermophysical Engineering **8**, pp341-359.

[6] Allen, M. P., and Tildesley, D. J., 1987, *Computer Simulation of Liquids*, Oxford University Press, Oxford, U.K.

[7] Ramsbey, M. T., Wolfe, J. P., and Tamura, S., 1988, "Phonon Focusing of Elastically Scattered Phonons in GaAs," Zeitschrift für Physik B **73**, pp167-178.

[8] Held, E., Klein, W., and Huebener, R. P., 1989, "Characterization of Single-Crystalline GaAs by Imaging with Ballistic Phonons," Zeitschrift für Physik B **75,** pp17-29.

[9] Bowman, K., 2003, *Introduction to Mechanical Behavior of Materials*, John Wiley & Sons, New York.

[10] Barker, J. A., and Klein, M. L., 1970, “Elastic Constants and Phonon Dispersion Curves for Solid Argon near 0 °K,” Physical Review B, **2** (10), pp4176-4179.